Alternative pathway for atmospheric particles growth

Maria Eugenia Monge[a], Thomas Rosenørn[a,1], Olivier Favez[a,2], Markus Müller[a], Gabriela Adler[b], Ali Abo Riziq[b], Yinon Rudich[b], Hartmut Herrmann[c], Christian George[a], and Barbara D'Anna[a,3]

[a]Université de Lyon; université Lyon 1; Centre National de la Recherche Scientifique (CNRS), unité mixte de recherche (UMR), 5256, IRCELYON, Institut de recherches sur la catalyse et l'environnement de Lyon, F-69626 Villeurbanne, France; [b]Department of Environmental Sciences, Weizmann Institute, Rehovot 76100, Israel; and [c]Leibniz-Institute for Tropospheric Research, Permoserstrasse 15, D-04318 Leipzig, Germany

Edited by Barbara J. Finlayson-Pitts, University of California, Irvine, CA, and approved March 9, 2012 (received for review December 13, 2011)

Credible climate change predictions require reliable fundamental scientific knowledge of the underlying processes. Despite extensive observational data accumulated to date, atmospheric aerosols still pose key uncertainties in the understanding of Earth's radiative balance due to direct interaction with radiation and because they modify clouds' properties. Specifically, major gaps exist in the understanding of the physicochemical pathways that lead to aerosol growth in the atmosphere and to changes in their properties while in the atmosphere. Traditionally, the driving forces for particle growth are attributed to condensation of low vapor pressure species following atmospheric oxidation of volatile compounds by gaseous oxidants. The current study presents experimental evidence of an unaccounted-for new photoinduced pathway for particle growth. We show that heterogeneous reactions activated by light can lead to fast uptake of noncondensable Volatile Organic Compounds (VOCs) at the surface of particles when only traces of a photosensitizer are present in the seed aerosol. Under such conditions, size and mass increase; changes in the chemical composition of the aerosol are also observed upon exposure to volatile organic compounds such as terpenes and near-UV irradiation. Experimentally determined growth rate values match field observations, suggesting that this photochemical process can provide a new, unaccounted-for pathway for atmospheric particle growth and should be considered by models.

atmospheric chemistry | photoinduced processes

Humankind is facing a changing environment, possibly due to anthropogenic stress on the atmosphere. In this context, aerosols play a key role through their influence on radiative climate forcing (1), the hydrological cycle (2), and their adverse effects on health (3). Organic material comprises a large fraction of the submicron aerosol mass, between 20–90% (4–6). The organic aerosol (OA) fraction is a highly dynamic system, tightly coupled to gas-phase oxidation chemistry (7). Atmospheric oxidation of gas-phase species by OH, O_3, NO_3, and Cl produce secondary organic aerosol (SOA) that accounts for a large fraction of the OA burden (6–10) and contributes to particle growth (11–14). Despite their importance, the processes leading to aerosol growth represent one of the most poorly understood topics in atmospheric aerosol science (15, 16). Models based on available parameterizations from laboratory studies underestimate the aerosol growth observed in the atmosphere (6, 8–10, 17), suggesting that unknown processes may exist. Results from this study challenge the traditional view of particle growth. An additional process is proposed: heterogeneous chemical reactions at the surface of organic particles, activated by sunlight, can lead to fast particle growth without need of gas phase oxidants in the system.

Experiments were performed using an aerosol flow tube reactor (Fig. S1) where a monodispersed aerosol was injected and exposed to a VOC either in the dark or under UV-A irradiation. Particle diameters were measured before and after the flow tube by means of a scanning mobility particle sizer (SMPS), while aerosol chemical composition was continuously monitored using an Aerodyne compact time-of-flight aerosol mass spectrometer (AMS—Aerodyne Inc.) (Fig. S1).

The VOCs used in this study were limonene and isoprene, as they are among the most commonly emitted biogenic species (18, 19). Seed particles were generated from an aqueous solution (pH = 5.6) of humic acid (HA), succinic acid and NH_4NO_3 (1:10:1 in weight). The relative humidity was 30%; i.e., under the experimental conditions the mixture was above the efflorescence point (20). The seed particles' composition is assumed to model the main features of (mainly organic) ambient aerosol, containing both complex and simple organics as well as inorganic components, possibly representing aged particles during long-range transport. HAs are considered to be proxy for atmospheric humic-like substances generated from biomass and wood burning because they have similar reactivity under irradiation (21–23). Dicarboxylic acids represent 4–15% of the total aerosol mass of atmospheric aerosol particles from continental and marine samples (24) and are formed from biomass burning, fossil fuel combustion, cooking, automobile exhaust, and atmospheric reactions of biogenic and anthropogenic VOCs (25). Field measurements deploying a single particle spectrometer, Aerosol Time of Flight Mass Spectrometer (ATOFMS), confirmed the presence of internally mixed particles containing organic carbon, ammonium, and nitrate (26).

Results and Discussion

Results from a typical experiment of seed particles exposed to 320 ppbv of limonene are depicted in Fig. 1. Size distribution and organic mass loading exiting the aerosol flow reactor remained constant under dark conditions. Under UV-A irradiation (3.7×10^{16} photons cm^{-2} s^{-1}, see Fig. S2), both mean diameter and organic mass loading rapidly increased (Fig. 1*A*), reaching a plateau after *ca.* 10 min (corresponding to the residence time in the flow tube). As soon as the light is switched off, the aerosol returns to its initial size distribution, underlining the photoinduced character of the process. Under irradiation, new fragment ions at higher m/z values appear in the mass spectra of the aerosol (Fig. 1*B*). The new fragments are identified as belonging to limonene itself and/or its reaction products, as they are only observed in presence of limonene. Control experiments indicate that no changes in particles size, mass and composition are observed during the dark experiments (Fig. 1*A*), suggesting that condensation of limonene does not occur and cannot explain the observed growth. Similarly, no changes in particle number and/or diameter are observed when the seed aerosol is irradiated in the

Author contributions: T.R., M.E.M., O.F., Y.R., H.H., C.G., and B.D. designed research; M.E.M., T.R., O.F., G.A., and A.A.R. performed research; M.E.M., M.M., H.H., and B.D. analyzed data; and M.E.M., G.A., A.A.R., Y.R., H.H., C.G., and B.D. wrote the paper.

The authors declare no conflict of interest.

This article is a PNAS Direct Submission.

[1]Present address: University of Copenhagen, Universitetsparken 5, 2100 Copenhagen, Denmark.

[2]Present address: INERIS, DRC/CARA/CIME, Parc Technologique Alata, BP2, Verneuil-en-Halatte, 60550, France.

[3]To whom correspondence should be addressed. E-mail: barbara.danna@ircelyon.univ-lyon1.fr.

This article contains supporting information online at www.pnas.org/lookup/suppl/doi:10.1073/pnas.1120593109/-/DCSupplemental.

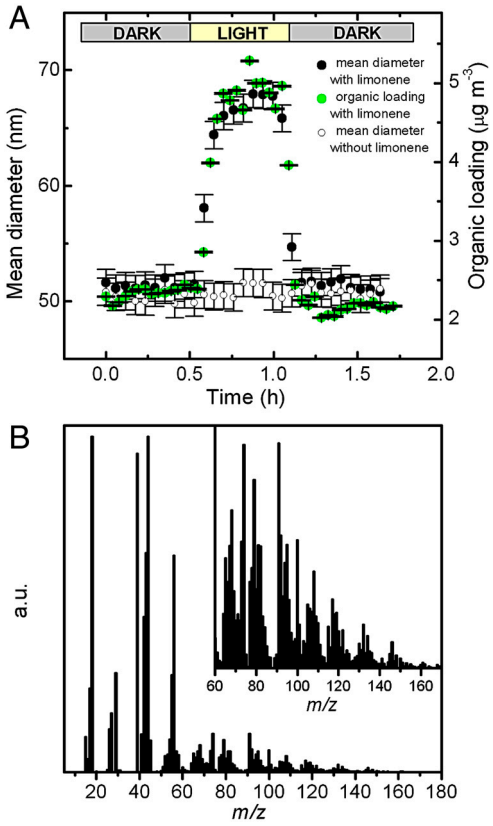

Fig. 1. Experimental results from an aerosol flow tube experiment using humic acid:succinic acid:NH_4NO_3 (1:10:1 in weight) as seed particles exposed to 320 ppbv of limonene and to UV-A light. The residence time of the aerosol in the flowtube is 9.7 min. (*A*) Mean diameter of the particles measured at the exit of the aerosol flow tube by SMPS (black dots) and total organic loading (green dots) measured by AMS. Particle mean diameter of a control experiment with no limonene in the gas phase is also shown (empty dots). Error bars correspond to 1σ. (*B*) Mass spectrum calculated by subtracting the averaged mass spectrum during irradiation from the averaged spectrum under dark conditions. The electron impact ionization energy was 30 eV to reduce fragmentation and improve the sensitivity to fragments with higher nominal mass. The insert is a zoom of the fragments with higher m/z values.

absence of the terpene, pointing out the absence of coagulation under the experimental conditions. Several control experiments were conducted as well; in one test, limonene alone was added to the carrier gas (air), and no new particle formation was observed under irradiation. In an additional control experiment, we used seed particles that contained only succinic acid. Under irradiation and in the presence of limonene, the mean diameter of the particles did not change. Similar results were observed for seed particles of pure ammonium sulphate. We therefore conclude that particle growth is observed only when the seed aerosol contains a photsensitizer (i.e., HA) exposed simultaneously to light and a gaseous terpene.

Replacing air by pure N_2 (containing up to 50 ppmv of O_2) reduced drastically the photoinduced particle growth (Fig. 2), suggesting that O_2 is involved in the reaction. The role of oxygen in the photochemistry of dissolved organic matter (DOM) and HAs is well known, and involves photosensitized reactions via singlet oxygen formation (27, 28). Direct evidence of photochemical generation of superoxide ion has also been reported in humic waters (29). Weak UV radiation carries enough energy to break chemical bonds in DOM to form free radicals (30). In addition, the carboxylate function of succinic acid and HA ($R-COO^-$) can act as an electron donor in charge transfer reactions with HA in its excited state (31, 32). Hydroxy radical (OH) formation may also occur in the particle through energy

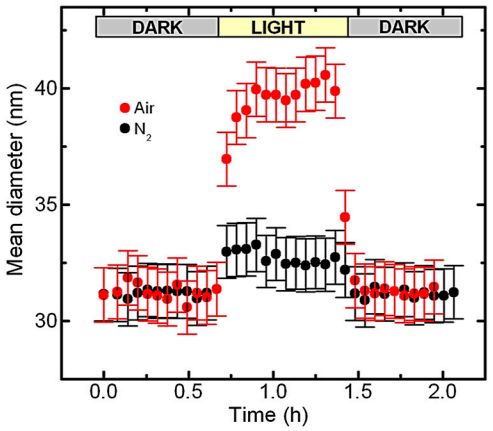

Fig. 2. : Changes in the mean particle's diameter for different carrier gas: N_2 (with 50 ppmv of O_2) and air. Seed particles of humic acid:succinic acid:NH_4NO_3 (1:10:1 in weight) exposed to 300 ppbv of gas phase limonene. Error bars correspond to 1σ. Residence time: 9 min.

transfer from the HA triplet state (33). Triplet state HA could also interact directly with the terpenes (34). The experimental observations suggest that the photoproduced radicals formed at the surface of the aerosol can possibly trap and oxidize terpenes (35) (Fig. S3). Addition of NH_4NO_3 to the seed particles slightly enhanced particle growth under irradiation. HA triplet state can react with nitrate anion through electron transfer reaction (29) and form a nitrate radical, which can be involved in the oxidation of terpenes and particle growth (Fig. S3). Control experiments using pure NH_4NO_3 aerosol do not show NO_x formation in the gas phase, suggesting that gas phase oxidants are not formed from NO_3^- photolysis under the chosen experimental conditions (36).

The first 1080 s of the plot shown in Fig. 1*A*, when the particles more than double their mass, were simulated using the COPASI software, which models acqueous phase reactions (37). It was assumed that equal amounts of NO_3 and OH form initially according to the conversions depicted in Fig. S3. At the onset of SOA production, a fraction of the OH and NO_3 radicals are converted into carboxylate-peroxyl radicals, which are assumed to also react with limonene and contribute to SOA formation. Due to the large turnover of the system, after 5 s all succinic acid species in the model aerosols are converted. From that stage on, the photogenerated species are expected to drive the SOA production without the involvement of succinic acid-derived radicals. COPASI modeling results indicate that two-thirds of the SOA are expected to form by a solution phase oxidation of limonene being taken up by OH and the other third by NO_3, possibly generated from particle nitrate. The overall particle growth predicted by the model is comparable with the experimental findings. Considering the particle growth shown in Fig. 1*A* at a light flux of 3.7×10^{16} photons cm^{-2} s^{-1}, an overall reactive uptake of $\gamma \approx 10^{-4}$ was estimated for limonene (see *Materials and Methods*). The exact elucidation of the particle phase chemistry taking place requires further detailed investigations of the reactions involved in separate bulk phase experiments.

The organic mass loading increases with the UV-A photon flux, as shown in Fig. 3*A*. Among the nominal masses involved, m/z 43.988, dominated by CO_2^+, is associated with the carboxylic functional group present in the seed particles. This fragment is stable both in the dark and under irradiation in the absence of limonene. Upon irradiation, m/z 43.988 increases, suggesting the formation of oxygenated products (Fig. 3*A*). Cumulative peak analysis of the mass spectra (38) indicates the presence of additional fragments. Among those, nominal masses m/z 80.062 and m/z 43.016, assigned to $C_6H_8^+$ and $C_2H_3O^+$, respectively, were highly correlated (correlation factor = 0.92). Fig. 3*B* shows their temporal evolution for normalized signals, at increasing photon

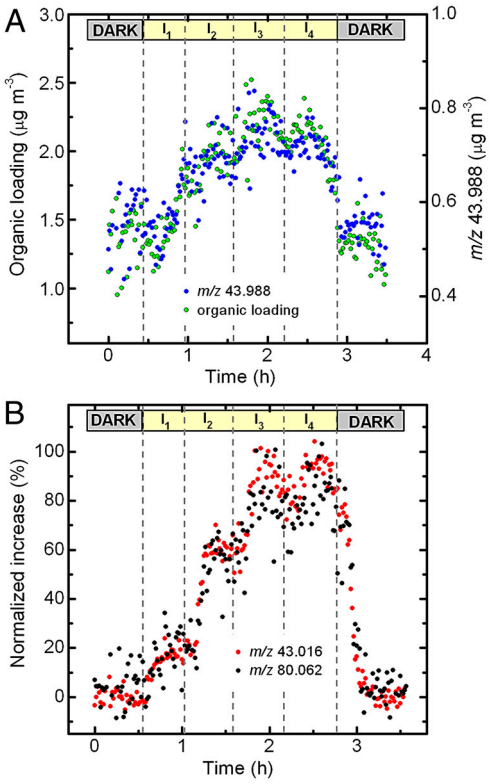

Fig. 3. Effect of light intensity on the organic mass loading and chemical composition. (*A*) Time evolution of the total organic loading (green dots) and of m/z 43.989 signal (blue dots) when seed particles of humic acid:succinic acid:NH_4NO_3 (1:10:1 in weight) are exposed to 335 ppbv of gaseous limonene at different light intensities. The upper box the dark-light conditions. I_i represent the different values of irradiance used ranging from 5.9×10^{15} photons cm^{-2} s^{-1} (I_1) to 3.7×10^{16} photons cm^{-2} s^{-1} (I_4). (*B*) Time evolution of the nominal mass m/z 80.062 ($C_6H_8^+$) and m/z 43.015 ($C_2H_3O^+$). Signals are normalized to their highest values. For simplicity, error bars are not shown.

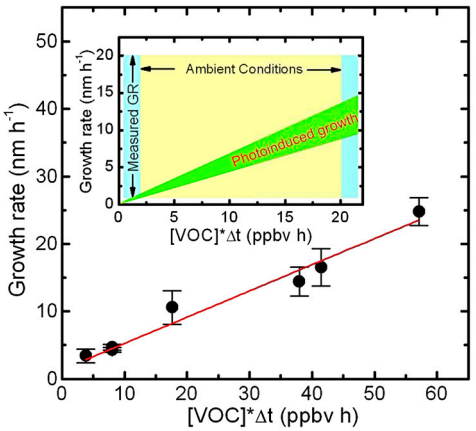

Fig. 4. Calculated growth rate values for seven experiments as a function of the product between limonene concentration and residence time in the flow tube. These values are calculated by considering the photoenhanced growth ($GR = \frac{\Delta D_m}{\Delta t}$) vs. VOCs concentration per exposure time. Values are evaluated for solar irradiance. The inset shows growth rate (GR) values given by the photoinduced process compared to the literature GRs values (1–20 nm h^{-1}). Ambient conditions are assumed to vary from 0.2 ppbv to 2 ppbv of limonene and exposure to solar irradiance for 10 h, in the 300–420 nm (near-UV) wavelength range.

flux densities. As m/z 80.062 is a typical fragment of limonene, its high correlation with $C_2H_3O^+$ indicates that both fragments arise from limonene reaction products (35, 39). Fig. 3*B* also shows that limonene is involved in the reactions leading to mass increase only under irradiation, as none of those signals are observed under dark conditions (condensation cannot therefore explain these observations).

Particle growth shows linear dependence on the photon flux in the 300–420 nm wavelength range (Fig. S4), doubling between the solar irradiance photon flux (1.9×10^{16} photons cm^{-2} s^{-1}) and the maximum experimental irradiance (3.7×10^{16} photons cm^{-2} s^{-1}). Furthermore, the overall size change depends on both limonene concentration and on the residence time in the flow tube (Fig. 4). Growth rate values ($GR = \frac{\Delta D_m}{\Delta t}$) are plotted as a function of the product between limonene concentration ([VOC]) and residence time (Δt); where ΔD_m is the difference between the mean diameter of the particles under irradiation (solar illumination: 1.9×10^{16} photons cm^{-2} s^{-1}) and the mean diameter in the dark. The linear dependence shown in Fig. 4 allows comparison of the experimental growth rates with those reported from atmospheric measurements in field campaigns; i.e., with 1 ppbv of limonene and 8 h exposure to near-UV light, a GR of 5 nm h^{-1} is observed. Data collected from more than 100 field studies indicate that typical atmospheric particle GRs (40) are between 1 and 20 nm h^{-1}, with remarkably constant GRs during daytime. The insert in Fig. 4 shows the expected GR values given by the photoinduced process presented in this work compared with the typical measured GRs (1–20 nm h^{-1}) under ambient conditions [mixing ratios of limonene between 0.2 ppbv to 2 ppbv (41) and 10 h of solar irradiance]. In addition, the insert shows that the photoinduced mechanism described in the present work may explain 70% of the maximum GR observed and agrees with the minimum GR reported within the experimental error. The GR values estimated in this work are consistent with those measured during field observations, suggesting that heterogeneous chemical reactions at the surface of OA can be activated by light and lead to efficient photoinduced mass transfer of VOCs to the aerosol phase. This process may be favored in different atmospheric environments, mainly for aged particles during long transport and far from their sources, and possibly for biomass burning plumes.

To assess the role of aerosols containing photoreactive compounds, additional experiments were performed using the aerosol flow tube in a stopped-flow mode and a quartz crystal microbalance (QCM). Isoprene was used as VOC and seed particles contained succinic acid and 4-(benzoyl)benzoic acid (10:1 in weight), a model compound found in biomass burning (42–46) also known to behave as a photosensitizer (31, 44, 47, 48). In the aerosol stopped-flow approach, the mass spectrum of the seed-isoprene mixture after irradiation shows new fragments formation at high m/z values when the seed particles are exposed to 900 ppbv of isoprene (Fig. S5*A*), and these signals are enhanced with increasing irradiation time (Fig. S5*B*). In agreement with the HA experiments, nominal mass m/z 44, representative of CO_2^+, increases as a function of the irradiation time and is almost constant in the dark (Fig. S5*C*). Similarly, the organic mass loading and the mean diameter of the aerosol increase immediately after turning on the lights in the presence of high VOC mixing ratios The signal returns to its initial dark phase value when the irradiation is turned off. These results suggest that oxygenated products form only in the presence of the UV light. It is important to highlight that without the photosensitizer, no high m/z signals are observed after 60 min of irradiation and no increase in the mass or mean diameter is achieved, underlining the key role of the photoactive compound in SOA growth and aerosol aging.

The QCM is highly sensitive to very small mass changes, and was used to study photoinduced mass transfer processes. A scheme of the experimental system is shown in Fig. S6. Shortly, a thin organic layer serving as a proxy for organic aerosols was deposited on a QCM placed in a temperature-controlled cell. The QCM was irradiated from the top by a UV lamp. The organic

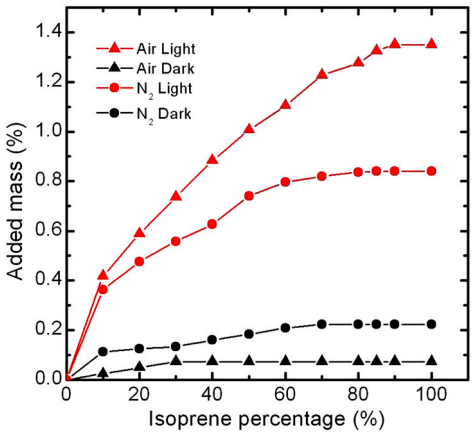

Fig. 5. Added mass due to isoprene adsorption on a layer of Nordic Aquatic humic acid mixed with succinic acid (1:10) deposited onto the QCM surface, representing the OA. The added mass is in percentage compared to the initial substrate at 0% isoprene vapor before and after 3 h of UV exposure for N_2 and air as carrier gas.

layer was composed of Nordic Aquatic HA mixed with succinic acid (1:10) or 2-benzoylbenzoic acid mixed with succinic acid and exposed to a stream of carrier gas (N_2 or air) seeded with a volatile organic (isoprene). Control experiments confirmed that under dark conditions, isoprene alone only slightly changes the resonance oscillation frequency of the quartz crystal (Fig. 5, Fig. S7). In the experiment with Nordic Aquatic HA, either N_2 or air was used as carrier gas (Fig. 5). Under UV irradiation the mass added to the layer increases by 1.35% using air as carrier gas and by 0.84% using N_2. These results support the aerosol flow tube observations (Fig. 2), confirming that oxygen plays an important role in the process. When isoprene is removed from the N_2 flow after dark exposure, the frequency of the QCM goes back to its original value, suggesting isoprene physisorption to the film; after irradiation, the QCM frequency does not return to its initial value, indicating that isoprene or its reaction products chemisorb to the layer. Similar results are obtained when 2-benzoyl-benzoic acid replaced HA (Fig. S6). The QCM experiments support the conclusions from the aerosol flow tube experiment; namely, that photosensitized processes enhance the mass transfer of terpenes to the organic matrix.

The results presented in this study suggest a new photoinduced mechanism for atmospheric particle growth. The newly identified pathway leads to aerosol growth by trapping noncondensable species, probably by photoinduced formation of radicals and singlet oxygen at the surface of the seed aerosol that can react with VOC impinging on the surface. The experimentally measured growth rates are consistent with those measured in many field studies, suggesting that photochemical processes can provide a new pathway for atmospheric particle growth and should be considered by models.

Materials and Methods

Aerosol Flow Tube. Experiments were conducted at atmospheric pressure in a horizontal cylindrical aerosol flow tube made of Pyrex (8 cm internal diameter, 152 cm of length); surrounded by seven fluorescent lamps (Philips CLEO) with a continuous emission spectrum in the 300–420 nm range and a total irradiance of 3.7×10^{16} photons cm^{-2} s^{-1} (Fig. S1). Temperature was kept constant at 293 ± 2 K using a circulating water bath through the outer jacket (Huber CC 405). Two different aerosol proxies have been investigated: *(i)* humic acid (Fluka), succinic acid (Aldrich) and NH_4NO_3 (Aldrich) (1:10:1 in weight) and *(ii)* 4-(benzoyl)benzoic (Aldrich) and succinic acid (1:10 in weight). Solutions were prepared using distilled 18 MΩ water (Millipore). The monodisperse aerosol was generated from an aqueous solution (pH = 5.6) by means of an atomizer (TSI Model 3076) and a SMPS™ TSI; impactor (nozzle size = 0.0508 cm, aerosol flow = 0.35–0.5 L min^{-1}, sheath flow = 10 L min^{-1}) (Fig. S2). Particle diameters of 30, 50, 80, and 100 nm were selected for analysis with the differential mobility analyzer (TSI Model 3081). The aerosol flow was initially dried with a Silica gel diffusion dryer and then mixed with a VOC, such as limonene or isoprene, whose flow was controlled by a permeation tube in a temperature-controlled enclosure (Dynacal, Valco Instruments Co. Inc.) using a VICI Metronics Dynacalibrator (Model 150). Seed particle concentration was approximately 4×10^4 particles cm^{-3}. Mixing ratios between 80 ppbv and 1 ppmv of limonene and between 600 ppbv and 800 ppmv of isoprene were used. Temperature and RH were measured at the inlet and outlet of the aerosol flow tube by a SP UFT75 sensor (Partners BV). Total flow rate values used: 0.5–3 L min^{-1}.

Upon exiting the aerosol flow tube, a portion of the aerosol was sampled by an Aerodyne compact Time-of-Flight (Tofwerk AG) AMS (Aerodyne Inc.) (Fig. S2). The AMS analysis provides a mass spectrometric fingerprint of the aerosol chemical composition (49). The aerosol is flash-vaporized at 873 K and ionized by electron impact at 30 or 70 eV. The low-energy ionization is used to decrease fragmentation and improve the observation of fragments with higher m/z. Finally, an ion guide transfers the positively charged ions into the compact orthogonal extraction Time-of-Flight MS. Spectral analysis was performed with Squirrel data analysis package (49) using a new methodology based on cumulative peak fitting and iterative residual analysis, which allows multiple isobaric peaks separation (38). Particle size distribution and concentration were measured using a SMPS consisting of a Differential Mobility Analyzer (TSI Model 3081) and a Condensation Particle Counter (TSI Model 3776).

Control experiments were carried out to determine the photostability of nitrate during the irradiated experiments of seed particles containing NH_4NO_3. A NOx detector (THERMO 42C chemiluminescent analyzer) connected to the aerosol flow tube exit did not detected any NOx species (detection limit of the instrumentation,0.4 ppbv) when monodisperse particles of pure NH_4NO_3 (50 nm diameter) were exposed to the near-UV lights for the highest residence time used in the flow experiments (16 min). In addition, O_3 production was checked using an O_3 monitor (Thermo 49C) and a FTIR cell. The results indicate that O_3 is not formed (detection limit is 1 ppbv for the ozone monitor and 40 ppbv for the FTIR-cell).

No particles formation was observed by the SMPS at the exit of the aerosol flow tube reactor when VOCs were irradiated for 16 min (absence of seed particles).

The aerosol formed by 4-benzoylbenzoic acid and succinic acid was studied using a stopped-flow approach, keeping the aerosol inside the reactor for different periods of time. When the system was stable in the dark, the flows were stopped and the lights turned on. Different irradiation times were examined (t = 20, 30, 45, and 60 min). After light exposition, the particles were analyzed by AMS. Similar experiments under dark conditions were performed to evaluate the evolution of the aerosol-VOC system at 30 and 110 min (Fig. S5).

Quartz Crystal Microbalance. Sorption was measured using a QCM (Stanford Research Systems, model QCM200, working frequency 5 MHz) consisting of a digital controller, a crystal oscillator, a crystal holder, a flow cell, and a quartz crystal sensor. Changes in the resonant oscillation frequency of the quartz crystal are proportional to changes in the crystal's mass according to the Sauerbrey equation $\Delta f = -C_f \times \Delta m$, where f is frequency in Hz, m is mass in g cm^{-2}, and C_f is the crystal sensitivity factor ($C_f = -56.5$ Hz μg^{-1} cm^2). For the Sauerbrey equation to hold, the sorbent layer deposited on the crystal must be thin, rigid, and with adherence. The sensitivity to mass change per sensor area can be as little as ±2 ng cm^{-2}, which is sufficient to monitor sorption on a thin sorbent layer, even when sorbent amounts are limited.

To create the sorbent layer, the crystal was precleaned with methanol, dried with N_2, and placed into the sensor-holder, which was then positioned into a flow cell held in a temperature-controlled water bath at 298.0 ± 0.5 K (Fig. S6). The null frequency (F_0), characteristic of a clean surface (no added mass), was obtained when 1 L min^{-1} of dry N_2 or air passed through the cell. Mixtures of Nordic Aquatic humic acid with succinic acid (1:10) and of 2-benzoylbenzoic acid with succinic acid (1:9) were dissolved in methanol/acetone (1:1) and methanol/hexane (1:1), respectively. The layer on the QCM surface was formed by depositing 3–5 droplets of these solutions and then evaporating the solvent with a N_2 flow. The system's performance was verified by measuring water adsorption on a Suwannee river fulvic acid layer at a different RH%. Wetting and drying cycles (0–90% RH followed by 90–0% RH at steps of 5–10% RH) were used to validate the system's performance (50). During conditioning, frequency and layer resistance were continuously monitored until reproducible water sorption and desorption curves were obtained, verifying the absence of any memory effect of the solvent. All QCM measurements were taken after frequency stabilization under UV irradiation; that is, the frequency change due to UV effect on the QCM crystal is already accounted for in the measurements performed under UV radiation

to allow comparison. In addition, all changes are presented in percentage from the initial value of the exposed crystal after several hours.

Sorption experiments involved continuous measurement of the frequency of the sorbent-coated QCM sensor while making stepwise changes in the flow cell gas phase composition at constant temperature (298 K). The coated sensor was exposed to increasing isoprene concentrations, with 5–10% increment steps from 0 to 100%. The effect of irradiation with UV light was studied at three wavelengths: 365.4, 404.7, and 435.8 nm (Fig. S6). Gas phase composition was controlled by mixing dry N_2/air and isoprene vapor-saturated N_2/air. The relative amounts of each component in the gas mixture were calculated on the basis of mass flow measurements using mass flow controllers (MKS Instruments, Inc.) calibrated before each experiment. The percentage of isoprene vapor saturated with N_2/air is dominated by the control of the N_2/air flow ratio of the N_2/air gas entering the system and the N_2/air gas entering the isoprene reservoir (at 238 K); the total flow of 100% is 1 L min^{-1}, and equilibrium was defined when the drift frequency was less than 1 Hz per hour.

Description of the Particle Phase Chemistry Model. A simple solution phase box model was set up applying COPASI (37). The model used the particle phase aqueous concentrations of succinic acid, nitrate, and humic acid as applied in the aerosol spray generator. OH and NO_3 production as well as limonene uptake were adjusted to mimic the measured SOA production in 1080 s. In total, 15 species and 13 reactions were implemented. NO_3 was allowed to react with the succinic species by single electron transfer followed by decarboxylation and addition of oxygen to form carboxylate peroxyl radicals. OH was allowed to react with the succinic species via H-abstraction, leading to dicarboxylate peroxyl radicals. Rate constants for these reactions were taken from available aqueous phase radical chemistry data. Both kinds of peroxyl radicals were allowed to react with limonene in the particle phase and to contribute to SOA formation, which also initiated by the direct reactions of both OH and NO_3 with limonene being taken up. To mimic the molar concentration of SOA being formed, a limonene SOA average molar mass of $M = 250$ g mol^{-1} was used.

ACKNOWLEDGMENTS. This work was supported by the Agence National de le Recherche Scientifique (ANR) under the Grant PHOTOAERO (ANR-08-JCJC-0093). Y.R. acknowledges support by the Helen and Martin Kimmel Award for Innovative Investigation. C.G. and Y.R. acknowledge support from NaBi, a CNRS-Weizmann Institute European Associated Laboratory (LEA). Support by the FP7 project PEGASOS (EU–FP7 project under *grant* agreement no. 265307) is gratefully acknowledged.

1. IPCC (2007) *Climate Change 2007—The Physical Science Basis: Contribution of Working Group I to the Fourth Assessment Report of the IPCC* (Cambridge University Press, Cambridge, United Kingdom).
2. Lohmann U, Feichter J (2005) Global indirect aerosol effects: a review. *Atmos Chem Phys* 5:715–737.
3. Donaldson K, Li XY, MacNee W (1998) Ultrafine (nanometre) particle mediated lung injury. *J Aerosol Sci* 29:553–560.
4. Kanakidou M, et al. (2005) Organic aerosol and global climate modelling: a review. *Atmos Chem Phys* 5:1053–1123.
5. Murphy DM, et al. (2006) Single-particle mass spectrometry of tropospheric aerosol particles. *J Geophys Res* 111:15–D23S32.
6. Zhang Q, et al. (2007) Ubiquity and dominance of oxygenated species in organic aerosols in anthropogenically-influenced Northern Hemisphere midlatitudes. *Geophys Res Lett* 34:6–L13801.
7. Jimenez JL, et al. (2009) Evolution of organic aerosols in the atmosphere. *Science* 326:1525–1529.
8. Goldstein AH, Galbally IE (2007) Known and unexplored organic constituents in the earth's atmosphere. *Environ Sci Technol* 41:1514–1521.
9. Hallquist M, et al. (2009) The formation, properties and impact of secondary organic aerosol: current and emerging issues. *Atmos Chem Phys* 9:5155–5236.
10. Heald CL, et al. (2008) Predicted change in global secondary organic aerosol concentrations in response to future climate, emissions, and land use change. *J Geophys Res* 113:D05211.
11. Boy M, et al. (2003) Nucleation events in the continental boundary layer: Long-term statistical analyses of aerosol relevant characteristics. *J Geophys Res* 108(D21):13–4667.
12. Kavouras IG, Mihalopoulos N, Stephanou EG (1998) Formation of atmospheric particles from organic acids produced by forests. *Nature* 395:683–686.
13. Laaksonen A, et al. (2008) The role of VOC oxidation products in continental new particle formation. *Atmos Chem Phys* 8:2657–2665.
14. Sellegri K, Hanke M, Umann B, Arnold F, Kulmala M (2005) Measurements of organic gases during aerosol formation events in the boreal forest atmosphere during QUEST. *Atmos Chem Phys* 5:373–384.
15. Wang L, et al. (2010) Atmospheric nanoparticles formed from heterogeneous reactions of organics. *Nat Geosci* 3:238–242.
16. Zhang R, Khalizov A, Wang L, Hu M, Xu W (2011) Nucleation and growth of nanoparticles in the atmosphere. *Chem Rev* 112:1957–2011.
17. Volkamer R, et al. (2006) Secondary organic aerosol formation from anthropogenic air pollution: rapid and higher than expected. *Geophys Res Lett* 33:L17811.
18. Geron C, Rasmussen R, Arnts RR, Guenther A (2000) A review and synthesis of monoterpene speciation from forests in the United States. *Atmos Environ* 34:1761–1781.
19. Guenther A, et al. (1995) A global-model of natural volatile organic-compound emissions. *J Geophys Res* 100(D5):8873–8892.
20. Lightstone JM, Onasch TB, Imre D, Oatis S (2000) Deliquescence, efflorescence, and water activity in ammonium nitrate and mixed ammonium nitrate/succinic acid microparticles. *J Phys Chem A* 104:9337–9346.
21. Baduel C, et al. (2011) Oxidation of atmospheric humic like substances by ozone: a kinetic and structural analysis approach. *Environ Sci Technol* 45:5238–5244.
22. .D'Anna B, et al. (2009) Light-induced ozone depletion by humic acid films and submicron aerosol particles. *J Geophys Res* 114:D12301.
23. Stemmler K, Ammann M, Donders C, Kleffmann J, George C (2006) Photosensitized reduction of nitrogen dioxide on humic acid as a source of nitrous acid. *Nature* 440:195–198.
24. Sempere R, Kawamura K (1994) Comparative distributions of dicarboxylic-acids and related polar compounds in snow rain and aerosols from urban atmosphere. *Atmos Environ* 28:449–459.
25. Schuetzle D, Cronn D, Crittenden AL, Charlson RJ (1975) Molecular composition of secondary aerosol and its possible origin. *Environ Sci Technol* 9:838–845.
26. Healy RM, et al. (2010) Source apportionment of PM2. 5 in Cork Harbour, Ireland using a combination of single particle mass spectrometry and quantitative semi-continuous measurements. *Atmos Chem Phys* 10:9593–9613.
27. Aguer JP, Richard C (1996) Reactive species produced on irradiation at 365 nm of aqueous solutions of humic acids. *J Photochem Photobio A* 93:193–198.
28. Latch DE, McNeill K (2006) Microheterogeneity of singlet oxygen distributions in irradiated humic acid solutions. *Science* 311:1743–1747.
29. Baxter RM, Carey JH (1983) Evidence for photochemical generation of superoxide ion in humic waters. *Nature* 306:575–576.
30. Sandvik SLH, Bilski P, Pakulski JD, Chignell CF, Coffin RB (2000) Photogeneration of singlet oxygen and free radicals in dissolved organic matter isolated from the Mississippi and Atchafalaya River plumes. *Mar Chem* 69:139–152.
31. Canonica S, Jans U, Stemmler K, Hoigne J (1995) Transformation kinetics of phenols in water—photosensitization by dissolved natural organic material and aromatic ketones. *Environ Sci Technol* 29:1822–1831.
32. de Semainville PG, Anna BD, George C (2010) Aqueous phase reactivity of nitrate radicals (NO_3) toward dicarboxylic acids. *Z Phys Chem* 224:1247–1260.
33. Vione D, et al. (2006) Sources and sinks of hydroxyl radicals upon irradiation of natural water samples. *Environ Sci Technol* 40:3775–3781.
34. Zepp RG, Schlotzhauer PF, Sink RM (1985) Photosensitized transformations involving electronic energy transfer in natural waters—role of humic substances. *Environ Sci Technol* 19:74–81.
35. Larsen BR, et al. (2001) Gas-phase OH oxidation of monoterpenes: gaseous and particulate products. *J Atmos Chem* 38:231–276.
36. Mark G, Korth HG, Schuchmann HP, vonSonntag C (1996) The photochemistry of aqueous nitrate ion revisited. *J Photochem Photobio A* 101:89–103.
37. Hoops S, et al. (2006) COPASI- A COmplex PAthway SImulator. *Bioinformatics* 22:3067–3074.
38. Muller M, George C, D'Anna B (2011) Enhanced spectral analysis of C-TOF Aerosol Mass Spectrometer data: iterative residual analysis and cumulative peak fitting. *Int J Mass Spectrom* 306:1–8.
39. Hamilton JF, et al. (2011) Investigating the use of secondary organic aerosol as seed particles in simulation chamber experiments. *Atmos Chem Phys* 11:5917–5929.
40. Kulmala M, et al. (2004) Formation and growth rates of ultrafine atmospheric particles: a review of observations. *J Aerosol Sci* 35:143–176.
41. Whitby RA, Coffey PE (1977) Measurement of terpenes and other organics in an adirondack mountain pine forest. *J Geophys Res* 82:5928–5934.
42. Anastasio C, Faust BC, Rao CJ (1997) Aromatic carbonyl compounds as aqueous-phase photochemical sources of hydrogen peroxide in acidic sulfate aerosols, fogs, and clouds. 1. Non-phenolic methoxybenzaldehydes and methoxyacetophenones with reductants (phenols). *Environ Sci Technol* 31:218–232.
43. Jang M, McDow SR (1995) Benz[a]anthracene photodegradation in the presence of known organic-constituents of atmospheric aerosols. *Environ Sci Technol* 29:2654–2660.
44. Net S, et al. (2009) Heterogeneous light-induced ozone processing on the organic coatings in the atmosphere. *Atmos Environ* 43:1683–1692.
45. Simoneit BRT, et al. (1993) Lignin pyrolysis products, lignans, and resin acids as specific tracers of plant classes in emissions from biomass combustion. *Environ Sci Technol* 27:2533–2541.
46. Vione D, et al. (2006) Photochemical reactions in the tropospheric aqueous phase and on particulate matter. *Chem Soc Rev* 35:441–453.
47. Canonica S, Hellrung B, Wirz J (2000) Oxidation of phenols by triplet aromatic ketones in aqueous solution. *J Phys Chem A* 104:1226–1232.
48. Net S, Nieto-Gligorovski L, Gligorovski S, Wortham H (2010) Heterogeneous ozonation kinetics of 4-phenoxyphenol in the presence of photosensitizer. *Atmos Chem Phys* 10:1545–1554.
49. Drewnick F, et al. (2005) A new time-of-flight aerosol mass spectrometer (TOF-AMS)—Instrument description and first field deployment. *Aerosol Sci Technol* 39:637–658.
50. Taraniuk I, Rudich Y, Graber ER (2009) Hydration-influenced sorption of organic compounds by model and atmospheric humic-like substances (HULIS). *Environ Sci Technol* 43:1811–1817.